Optical characterizations of falling droplets interacting with shock wave

Pierre Slangen, Pierre Lauret, Laurent Aprin, Frederic Heymes, Nicolas Lecysyn

Optical characterizations of falling droplets interacting with shock wave

Pierre R. Slangen[1,*], Pierre Lauret[1], Laurent Aprin[1], Frederic Heymes[1], Nicolas Lecysyn[2]

[1]Institute for Risk Sciences, LGEI, Ecole des Mines d'Alès, 30319 Alès Cedex, France
[2] CEA Gramat, BP80200, 46500 Gramat, France
*corresponding author: pierre.slangen@mines-ales.fr

Abstract Optical diagnostics are commonly used for imaging and/or measuring with accurate temporal and spatial resolutions. Huge frame rates impose short exposition time and high sensitivity sensors. These recording sensors are typically impinged with important light flux from specialized or dedicated light sources such as super bright LED array.
Risk sciences involve different phenomena including explosions, fires, brittle fractures or high speed impacts and interaction of fluids with shock waves.
The aim of this paper is to characterize the interaction of falling droplets with shock waves. At the laboratory scale, the presented device is made of a horizontal shock tube releasing blast or shock wave from the rapid rupture of a disc around 4bars. Shock wave is propagating and guided by a secondary tube and then impacts falling droplets of e.g. water. We present the optical measurements of this set-up concerning the speed and shape of the shock wave and droplet interaction by using direct shadowgraphy at the droplets jet scale. In this case long range macro objective have been used, lateral resolution is 65µm/pixel for 63mm*21mm region of interest. Larger scale study (about $1m^2$) is realized by retroreflective Edgerton shadowgraphy also called Pure In Line Shadowgraphy (PILS). Large scale and drops scale measurement have been realized in the same time by using 2 high speed imaging cameras. Optical measurements are coupled with high speed pressure sensors to ensure complete shock wave characterization.
Effects of the generated shock wave on the droplets are shown. Results are presented and discussed through PIV/PTV analysis.
Keywords: high speed imaging, droplets, shock wave, pure in line shadowgraphy

1 Introduction

Flying fragments, shock waves and high heat radiation can occur in industrial accidents involving successive explosions. Impacting a tank of low flammable and/or hazardous liquid in conventional storage conditions can generate loss of containment of the product. The leak is commonly ejected in the surrounding atmosphere in the form of big liquid droplets or filament [1]. Krishna [2] mentioned these droplets have an important probability to disperse over a significantly larger area than the bulk liquid. In addition, the interaction of this two phase jet with a shock wave, coming from another explosion (e.g. in domino effect), may reach the atomization of these big drops involving dispersion of toxic or flammable cloud. The characterization of these interactions are then of first interest in the risk sciences [3].
Previous paper of the authors [4] concerned the interaction of high speed air flux with falling droplets. In this study, they have shown the applicability of time resolved shadowgraphy by using PLIF (Pulsed Laser Induced Fluorescence) light source coupled with high speed imaging camera to characterize the interaction of the high speed flow and the droplets at small scale (20mm*20mm ROI). Results showed the effect of the flow speed and the influence of the physicochemical properties of the droplets liquid.
Since then, a brand new shock wave generator has been developed and equipped with high speed sensors to record the pressure variations, inside and outside the open-ended shock tube. Moreover dedicated pressure sensors have been used to measure accurately the shock wave speed in different locations.
On the optical point of view, the main problem for this kind of applications is the frame rate of the imaging sensors to record the different stages of droplet evolution during the shock and also to fully characterize the shock wave in lateral extension. In [4], authors used PLIF light source from a double cavity 15mJ-10ns pulsed Nd-YLF laser impinging doped polymer to generate a 10cm diameter collimated beam of yellow incoherent light. This system can deliver double pulse of up to 15mJ at 4.5kHz synchronized with high speed imaging camera in PIV (Particle Image Velocimetry) mode. This implies the camera burst mode enabling to drive the electronics so as to get the maximum double frame rate. In the case of high speed imaging, double frame means the recording of two successive images separated by, at least, the straddle time of the camera.

Straddle time is the minimum time required to read and purge the frame grabber and makes it ready for a new image acquisition. The number of images in the burst and the burst frequency is “only” limited by the frequency bandwidth of the camera. So the limit of Time Resolved PIV (TRPIV) with PLIF source is then limited by straddle time and bandwidth of the camera and the refreshing time of the laser cavities, including Q-switch delay and light delivering. This implies a careful time synchronization of the different components of the set-up.
The final charged bill for time resolved measurement is very often the spatial resolution and so forth the scale of the measurement. In the meantime shadowgraphy implies parallel beams or collinear beams between lighting source and observation sensor. This is strongly affecting the range of observations to some tens of centimetres if large and costing lenses or mirrors have to be avoided. Some authors presented high speed Edgerton retroreflective shadowgraphy [5] refreshed to cope with large scale measurement of explosions and gunshots [6, 7]. For simplicity reason, we suggest to use this Pure In Line Shadowgraphy (PILS) instead of Edgerton reflective shadowgraphy.
The coupling of local shadowgraphy in the vicinity of the droplets and PILS enables to jump in the magnification range and so to collect information with time and spatial resolutions when needed. It is kind of multiplexing the recording system thanks to 2 high speed imaging cameras (7000fps, 12 bits 1280*960 pixels).

2 High speed imaging

Time resolved measurement requires high speed framing devices. Two different categories of high speed imagers can achieve these performances: CMOS sensors with associated Rolling Memory Buffer (RMB) and In Situ Image Storage (ISIS) sensors (CCD or µCMOS) with local image storage. These sensors are commonly used with different kind of lightings e.g. LEDs, laser or metal vapour lamps.

2.1 CMOS sensors and Rolling Memory Buffer (RMB)

CMOS RMB device are now reaching up to 25000fps/s, 12 bits 1 Mpixels (PhantomV2511, Vision Research) with straddle time as short as 293ns (Photron SA-Z, Photron). Spatial resolution is achieved with thousands of pixels from 20µm to 28µm size resolution to reach the required light sensitivity (up to 32000 D monochrome ISO 12232 SAT). The other advantage of the CMOS RMD is the possibility to enhance frame rate by reducing image resolution. For some sensors this can only be done mainly in one direction and so just request tilting the sensor head by 90 degrees. Finally, rolling buffer memory (Fig.1) enables triggering the acquisition from passive (rewriting the buffer in FIFO, pre-trigger) to active or live images (keeping an amount of passive images before trigger and active acquisition after trigger in the post-trigger buffer).

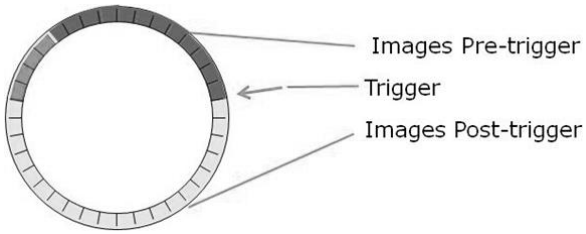

Fig. 1 Triggering the rolling buffer memory

Huge RMB up to 96GB enables long sequences recording. Cameras are commonly remote-controlled by GigE RJ45 cables or so and transfer the RMB content to external storage devices up to 10Gb/s (UHS SD memory card, SATA disk) or more for dedicated SD drive (Cinemag®). Some manufacturers even enable driving focus and zoom of the coupled lenses.

2.2 ISIS sensors

ISIS sensors have dedicated architecture to enable ultrafast transfer at “electron speed” from the collecting image area to the storage areas. This architecture stores the next images nearby the collection image sensor with high resolution but is really sensitive to noise or blooming. The bloomed live image can sometime flow

in the stored neighbored images and bloom it. But the main advantage is to get ultra-high speed up to 200Mfps with this kind of sensors (1000*860 pixels, 24 frames, Hadland UHSI). As 200Mfps requires at least 5ns of exposure, the sensor must be really sensitive or the lighting must be very efficient…without frying the object. As the storage areas must be close to the collection area, the number of stored images is really low (up to 200 frames, Shimadzu HPV or Specialised-Imaging Kirana) for relatively good resolution (924*768 pixels, Kirana). The major con is then the camera trigger synchronization with the event under investigation. The period of measurement is also as short as the number of stored images times the frame rate…

2.3 Light sources

Lighting the object to get short exposure time to freeze the object movement is the major rule. But rule number one is really "don't fry the object". In classical imaging, some black carbon-reinforced spatial container can rise up to 80°C in less than 60seconds when lit by powerful 4kW HMI (Hydrargyrum (mercury) Medium-arc Iodide) spots. This kind of lighting is now commonly replaced by Super Bright LEDs gratings reaching up to 18klumen (of "cold" light) for only 300W consumption or less. If high power point source is needed, it is also possible to use Xe or Xe-Hg arc lamp.
For dedicated imaging like shadowgraphy and schlieren, SB LEDs are also used and will progressively replace pulsed laser for low pulsed rates. On the other hand, pulsed laser are now reaching 20kHz rates of 100mJ pulse in the green line (527nm fd-NdYLF or 532nm fd-$NdYVO_4$ where fd denotes frequency doubling). Double or triple pulses can be generated by associating multiple cavities and triggering the laser emission with respect to the optical sensor head. The effective cost of laser light is the laser safety running with the laser system (laser goggles, curtain, light sign, door switch…) but the worst case in high resolution imaging is the speckle generation. Even if PIV lasers have bad light coherence, the speckle always appears. Therefore these lasers are very often coupled with polymer plates doped with dyes and so generating Laser Induced Fluorescence (LIF) when lit by the laser beam. This contributes to rise the Modulation Transfer Function of the optical system from coherent to non-coherent and insures image sharpness, free of speckles and secondary interference fringes when using Fresnel collimator or light sheet generator. For very short pulse duration and PIV mode camera acquisition (the camera exposure is kept "open" within the frame rate and the pulse duration is the exposure time), lasers stay the best source to freeze the object. For multiple pulse imaging, the limiting factor of two consecutive frame is the straddle time (Fig.2) of the camera, and the repetition of the pulses burst (>2 pulses) is given by the recording bandwidth of the camera.

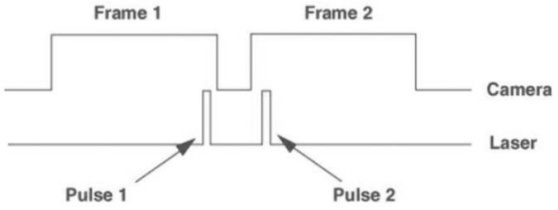

Fig. 2 Straddle time between pulse 1 and pulse 2

3 Experimental methods

As already expressed in section 1, the main goal of this paper is to assess the behavior of falling droplets rocked by incident shock wave with dedicated optical techniques. This interaction can lead to different atomization modes described by Lee *et al* [8] and more recently by Lin and Ruschak [9]. The main parameters for the breaking modes are ρ_g and ρ_l the gas and liquid densities, σ the surface tension of the liquid, u_g the velocity of the air flow, μ_l the viscosity of the liquid and D_0 the initial diameter of droplet before disintegration. This enables to compute adimensional number such as the Weber number (balance of dynamic pressure by surface tension pressure) or the Ohnesorge number (balance of viscous forces by inertial and capillary forces):

$$We = \frac{\rho_{g(\Delta u^2)D_0}}{\sigma} \qquad Oh = \frac{\mu_l}{(\rho_l D_0 \sigma)^{1/2}} \tag{1}$$

To fill the different data request from the falling drops impacted by shock wave, the shock wave generating tube will be described. Two different set-ups have been used.
The first set-up uses two high speed cameras placed in direct shadowgraphy with focus on the drops for the first camera and in PILS configuration to show the shock wave propagation for the second camera.
The second set-up enables to measure the pressure variation outside the shock tube and also the speed of the shock wave with dedicated pressure sensor. The different sensors are connected to HBM Genesis Gen7 high speed acquisition board delivering pre and post trigger signals. The main trig is realized through variable sound sensing probe delivering 5V TTL signal directly to the cameras and Genesis board. As the frame rates of the cameras are different, there is no need of internal frame rate synchronization between the two.

3.1 Shock tube

The device generating the shock wave is made of steel with an inside diameter of 15cm. The whole tube is about 2.36m and divided in three pieces (high pressure chamber, rupture membrane and side flaps, release tube). The first chamber is 30cm long and closed on one side. The other side is free and can be closed by a rupture membrane the dimensions and material of which drive the pressure rupture (e.g. 4.2 bars for 2/10mm thick aluminum). This pressurized chamber is hermetically linked to a 2m long parallel tube. The droplet generator is placed at the exhaust of this secondary tube so as the drops are free falling in front of the shock wave without purging the droplet pipe by dynamic depression. The shock tube is equipped with different sensors (Fig.3) to record e.g. temperature and - PCB type M102A06 - dynamic pressure transducer at different points. Theses sensors are connected to fast data acquisition HBM Gen7, synchronizing all data's, image acquisition and triggering (peak detection from pressure sensors OR external sound trigger OR manual trigger) at 250kHz sampling.
Pressure sensor C1-28810 is fed directly in the tube nearby the inner surface and gives the pressure variation just before the tube outlet.
Pressure sensors C2-28018 and C3-28016 are placed on the same free-field blast pressure rod and separated by 100mm. This home-made configuration rod enables measuring the exact speed of the shock at 310mm of the tube outlet. The rod has been machined to avoid any reflection of the shock.
Sensor C4-7074 is placed on a single rod and measure the reduced field pressure at 5m of the tube outlet. First tests have been carried on to determine safety distance for optics and cameras.

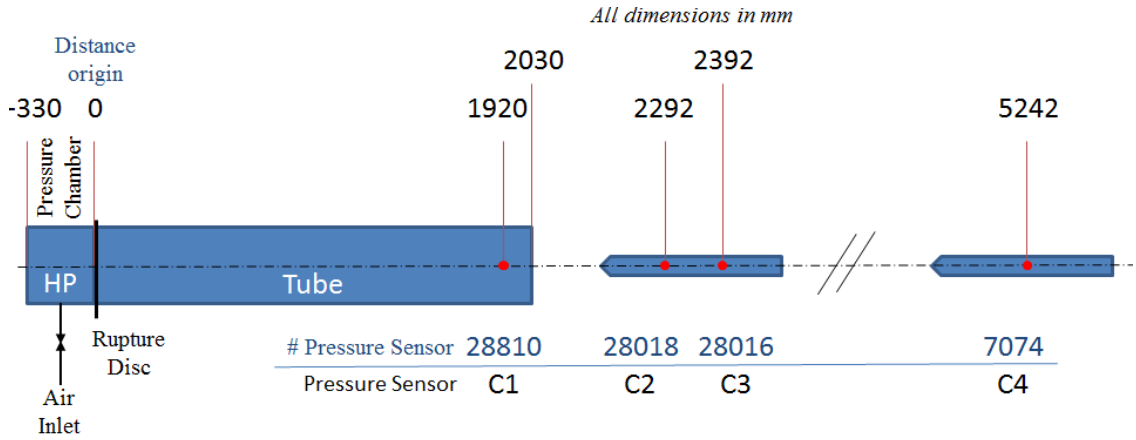

Fig. 3 Shock tube configuration with sensors

3.2 Optical measurements

The desired measurements require recordings of both zoomed view on the drops and larger view to characterize the shock wave geometry and speed. Moreover, this large view also enables to record the interaction of secondary reflexions with already "dispersed" drop fragments (see infra). As the measurements must be time resolved, powerful lighting has been used to reach short exposure time and frame rates higher than 15kfps. Phantom V711 camera bandwidth is 7Gpix/s and take 7530fps 12bits-depth 1280*800 pixels, 25000fps at 512*512 pixels… and up to 1 400 000fps at 128*8 pixels, with 293ns smallest exposure time.

3.2.1 Direct shadowgraphy

Direct shadowgraphy is completed by using backlighting of the droplets with collimated light beam.
The zoomed view is achieved through mounting fast camera 12 bits Phantom V711(V711S, S for Shadow) with Tamron 70-300mm f/4-5.6 zoom lens, in front of direct illumination from superlum LED array (Veritas Constellation 120, 18klm continuous). This high efficiency light source is really comfortable using as it just required 300W and delivers as much flicker-free light as 2.5kW HMI projector. This lighting is shone directly into the zoom aperture.
V711S is running at 22kfps, 320*960pixels reduced resolution with exposure as short as 294ns to freeze the droplet motion. The field of view given by Tamron 300mm f/5.6 lens is about 21mm wide by 62mm long to cope with droplet horizontal motion from the shock. The geometric calibration gives 65µm/pixel (Fig.4).

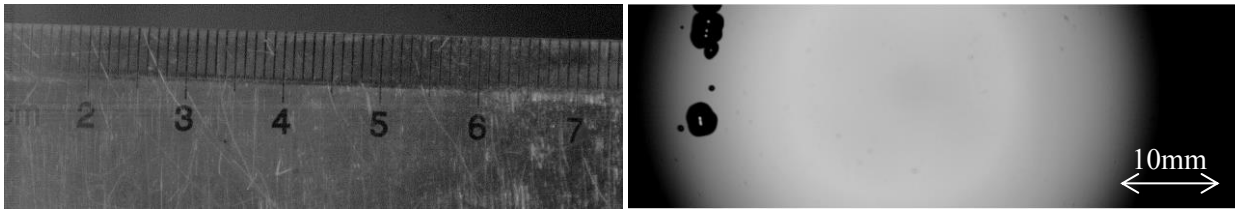

Fig. 4 Direct shadowgraphy: Calibration and falling droplet images

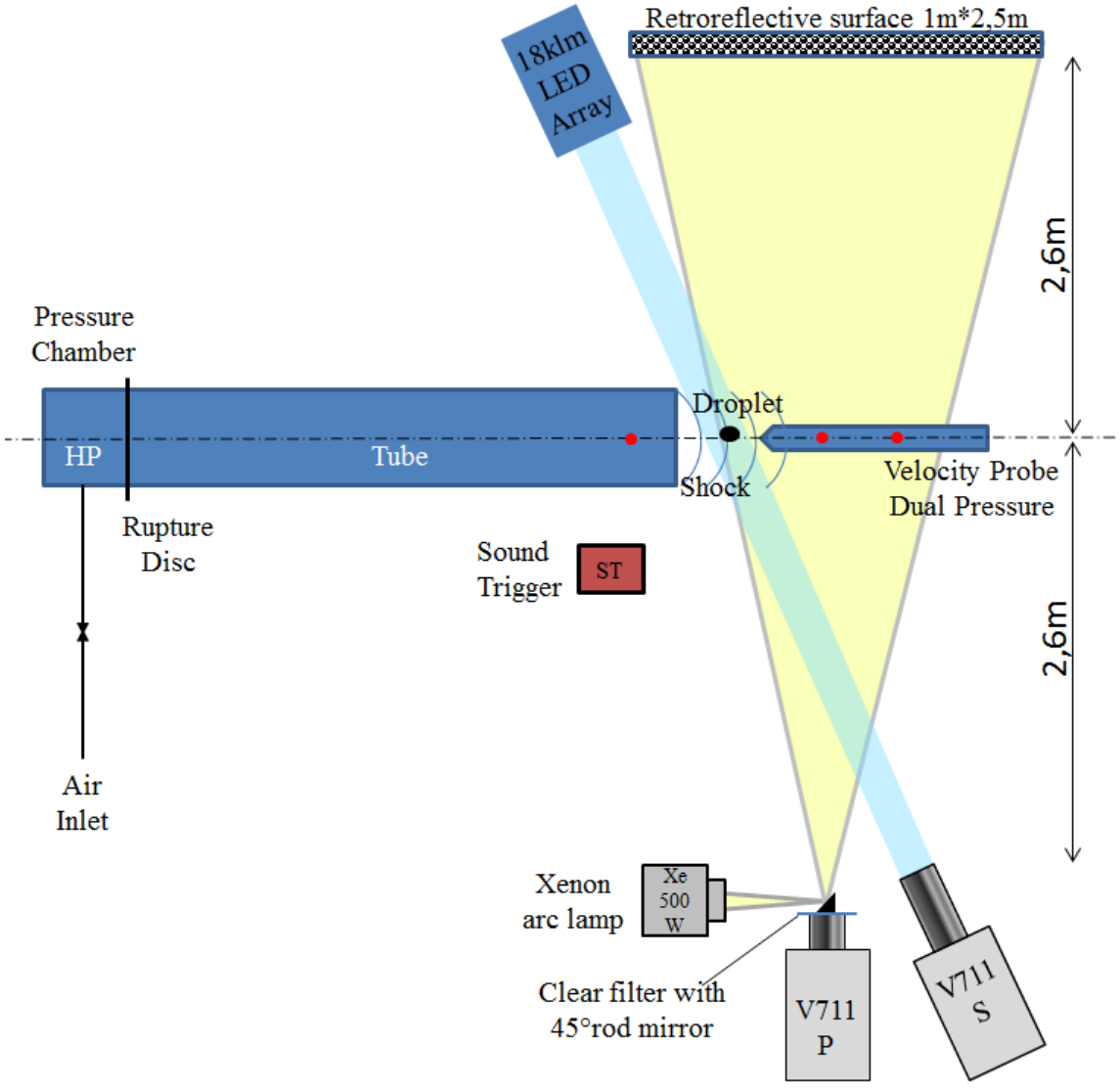

Fig. 5 Shock wave tube and optical set-up's: PILS and direct shadowgraphy

Previous works [4] have shown using double pulse PIV enables short time between pulses but require some laser and camera delays so as to refresh laser cavity or wait for next burst limited by camera bandwidth. This limitation is 4552 double fps with Phantom V711 in PIV mode. Therefore the option of single frame free run with higher frame rate has been preferred. The freeze of the secondary droplets is then reached by 293ns exposure time instead of 10ns laser pulse, which is enough for the expected velocities. The superlum light flux is also much more important than the one from Xenon lamp for PILS reflected by the drops. There is no interference between these two methods even if both are in "white" light with crossing spectra.

3.2.1 Pure In Line Shadowgraphy - PILS

As above-mentioned, we have chosen to gently rename retroreflective Edgerton shadowgraphy into Pure In Line Shadowgraphy (PILS). Hence the acronym is closer to (TR-SR)PIV, PLIF, LIF, DIC… and also enables us to acknowledge "Doc Edgerton" giving us the right pill removing the researcher's headache while chasing after large field shadowgraphy solutions ;-). The final collinear solution has been carried on by Settles et al [7].
To cope with large field of view, PILS set-up is integrated in the same area to get droplet view and shock propagation (Fig.5). So the second Phantom V711 camera (V711P, P for PILS) is used to record the PILS signal from the retroreflective surface (Orafol, Oralite5300 Reflective Film). This adhesive film is made of catadioptric glass beads embedded in a transparent layer of plastic material. The specific coefficient of retroreflection R' is about 50 cd/lx/m2 for 0.2° angle of observation, and entrance angle less than 5°.
V711P is running at 20kfps, 752*400 pixels reduced resolution with 10µs exposure time. The field of view of the Nikon 50mm f/4, in the droplet space, is about 336mm wide by 630mm long to cope with droplet horizontal motion from the shock. The geometric calibration gives 840µm/pixel at the velocity probe dual pressure sensor (C2-C3) plane (Fig.6).

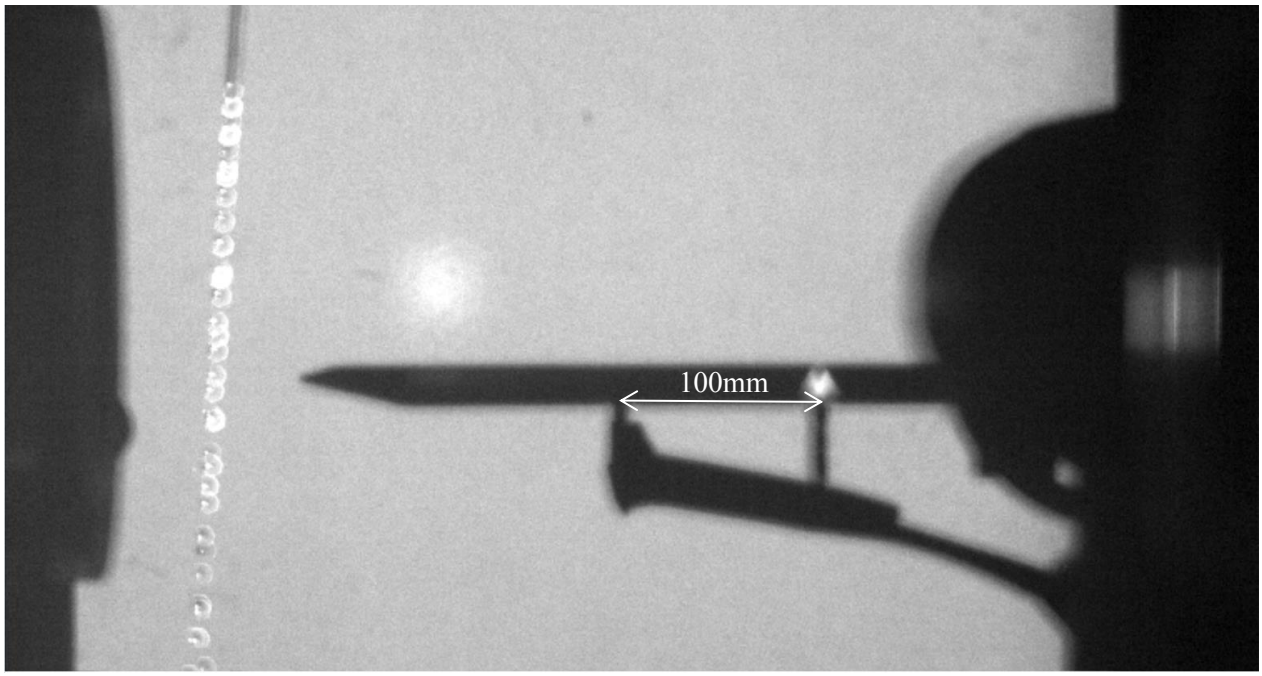

Fig. 6: PILS image of falling droplets before shock

As shown by Fig.5, PILS set-up involves the exact collinearity of source beams and reflected beams after passing through the region of interest. Light flux from an arc lamp (Newport, Hg-Xe, 500W) is focused on a 4mm diameter 45° rod mirror. The rod mirror is cemented to the center of a clear filter mounted in front of the V711P camera objective (Nikon 50mm, f/1.4 lens). Collinearity between the beams is reached as the emitted beams from the rod mirror are exactly back-reflected by the 1mx2.5m reflective screen. The screen is located at the same distance from the drop generator as the camera lens. All not-disturbed light is reflected straight backward while shadow or perturbed light is not. Thus the equidistance between camera-drop and drop-screen ensures a perfect match of the direct image with the shadow image, as the balance of

magnification is the balance of distance. Focus of the camera lens is done on the shadow screen. To collect enough light for small exposure time, without being fuzzed by rod mirror, wide apertures must be selected while closing aperture to enhance depth of field decreases drastically light flux. Good balance is reached by f/8 aperture. But as the working distance is 2.6m, the depth of field is not long enough to show sharp object and shadow images even with 50mm focal length. The final choice of the objective lens and the focused angle of the light beams from the arc lamp is directed by the working distance, the ROI surface and the camera sensitivity. Moreover, for speed acquisition higher than the nominal acquisition speed, the focal length must be selected to show the desired ROI at reduced camera sensor resolution.

4. Results

The shock tube is working through the rupture of an aluminum membrane placed between the high pressure chamber and the guiding tube. We have first tested the pressure rupture and the generated shock wave. Droplets have then been injected for final measurements and characterization.

4.1 Shock wave geometry and velocity

The shock wave can be described in terms of velocity and geometry. This geometry can evolve with the distance from the outlet. Different tests have been carried on to select the right membrane configurations (thickness and material). Figure 7 presents the main phases of the wave evolution by PILS. Plane wave (1D) from the inner tube is diffracted and evolves as circular wave (3D).

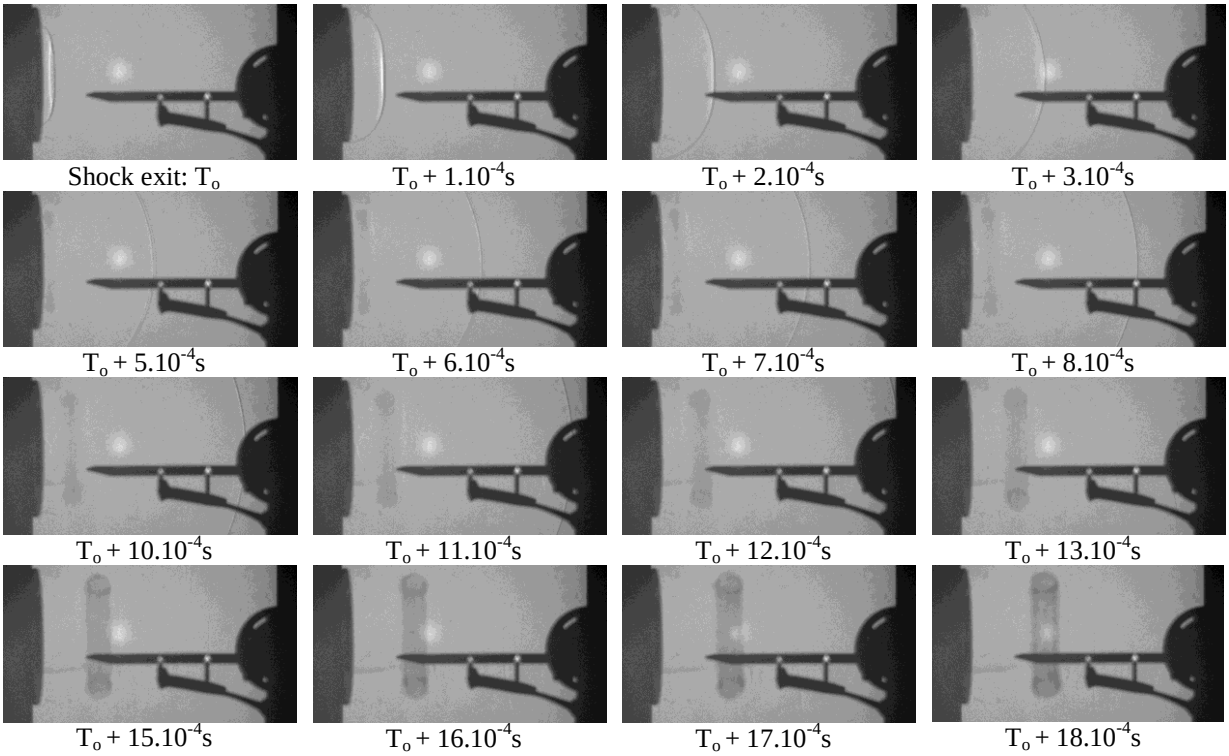

Fig. 7: Shock wave propagation and vortex

The shock velocity is around 436m/s and decreases with distance to 360m/s after sensor C_3 (Fig.8). The x-axis plot in second is linked to the image time-stamp, and so the position of the shock wave. These results have been confirmed by comparison with the velocities values obtained from the pressure transducer. Fig.9 presents the pressure transducer signals used to get the velocities between transducers C_2-C_1 and C_3-C_2 (white rectangle), i.e. 442m/s and 357m/s, respectively. These signals also show secondary and reflected shock waves clearly visible on the PILS images but not presented here to save some space.
Also shown Fig.7, circular wrapped vortex is exiting the tube 0.5ms after the first shock and propagates at about 165m/s.

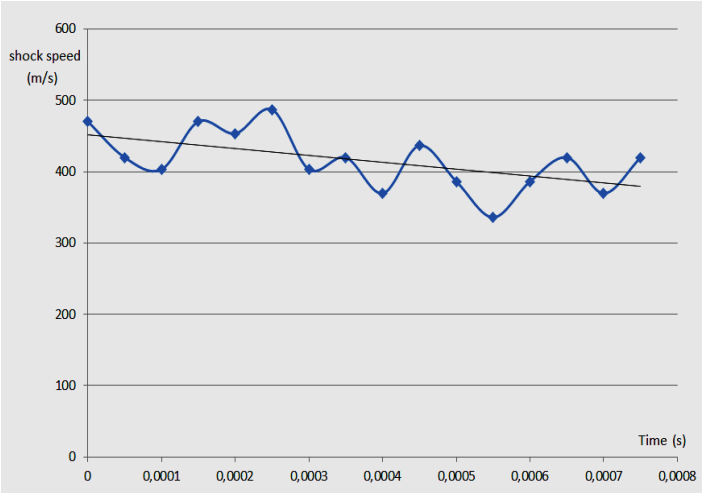

Fig. 8: Evolution of the shock velocity (from Fig.7, V711P images)

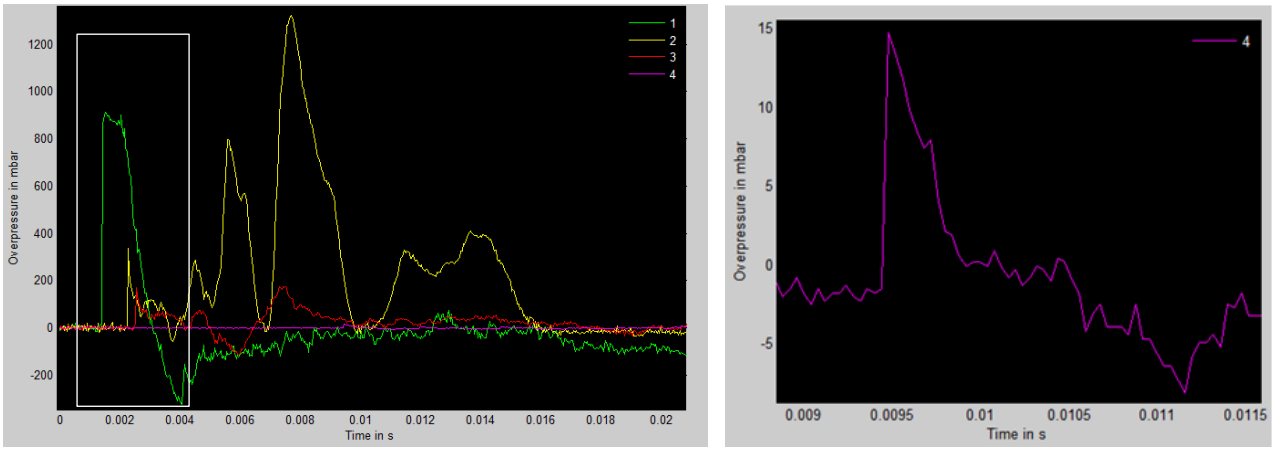

a) All sensors signals and zoomed C4 signal (0.009s, 0.011s)

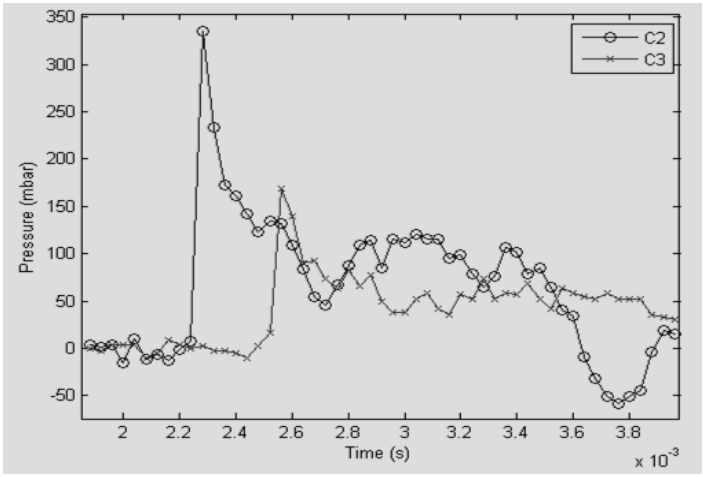

b) C_2, C_3 zoomed signals

Fig. 9: Pressure transducers signals

This set of measurements enables the validation of the shock tube and also using PILS as shock wave detection. The aluminum membrane is cut from aluminum roll and always placed in the same orientation following the calender direction to ensure reproductive strain direction and pressure rupture up to 4.2bars between the high pressure chamber and the tube.

4.2 Droplet and shock wave interaction

After calibration of the set-up described in the previous section, the droplet generator has been added to the exit of the tube. The droplet generator is made of automatic syringe pusher filled with the liquid under study. The syringe is connected to a 3mm rigid pipe placed on the top of the outlet tube with an independent holder. The distance between the pipe tip and the tube is 85mm, centered and 15cm height from the tube axis. Continuous drops train ensures the interaction of falling drops with the shock wave as trigging the rupture is not enabled.
To measure accurately the droplet shift and behavior, the direct shadowgraphy (DS) system has been added. DS also enables to visualize the shock wave in the vicinity of the droplet. Consecutive frames are presented each 1/22006s separated (Fig.10). It is then possible to characterize the behavior of the droplet interaction with the shock wave in a large area of interest, with different lateral resolution and nearly at the same frame rate.

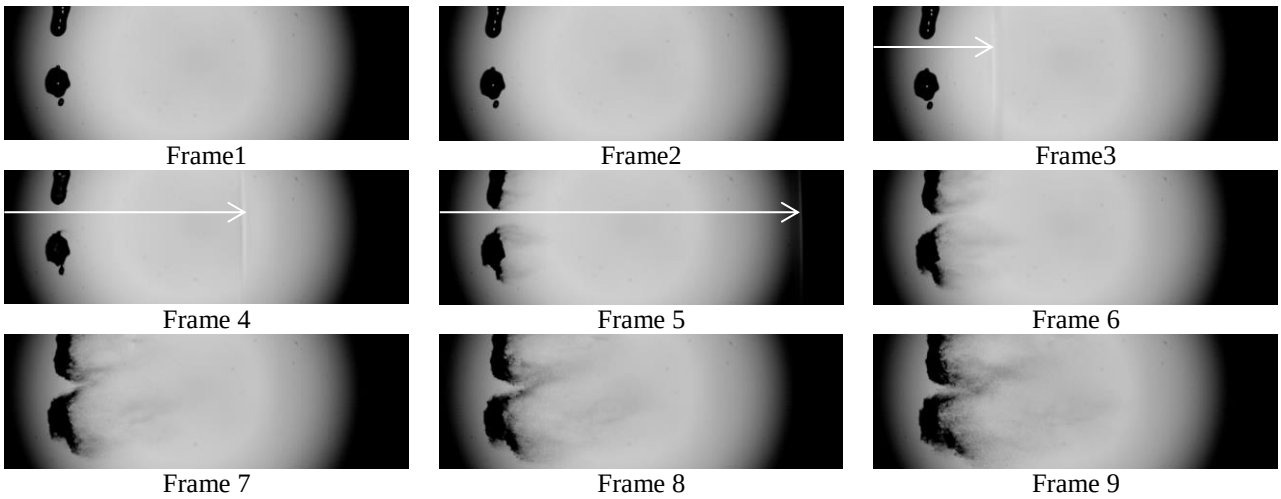

Fig. 10: Consecutive direct shadowgraphy frames (1/22006s separated)

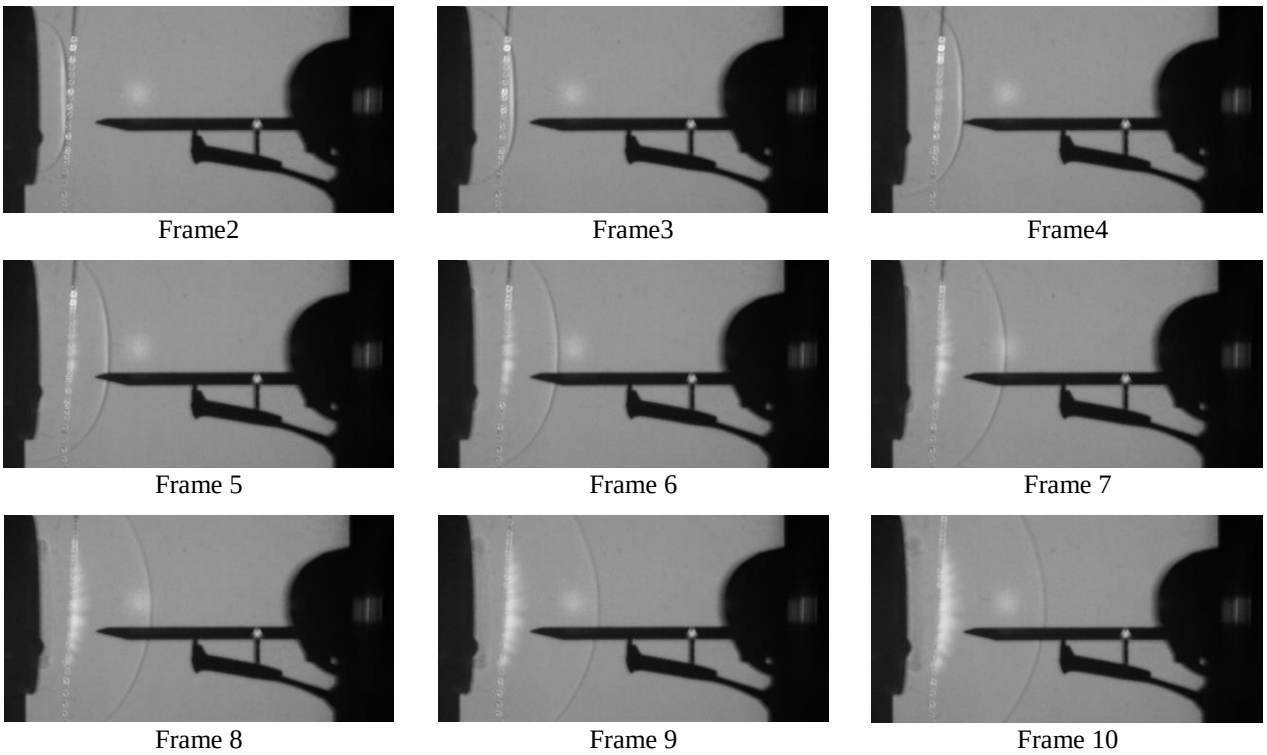

Fig. 11: Consecutive PILS frames (1/20000s separated)

The shock is clearly visible in direct shadowgraphy and the distance between the two shocks in Frame 3 and Frame 4 (and also Frame 5 in lower bits image) leads to shock velocity of 406m/s. The interaction of the shock and the droplet is detected on Frame 4 with the beginning of stripping and catastrophic breakup.

The same region of interest is also recorded by the PILS set-up as shown Fig.11 (synchronization "+1 frame"). With lower lateral resolution, the shock velocity is around 420m/s, which is in good agreement with DS and average pressure transducer velocity.

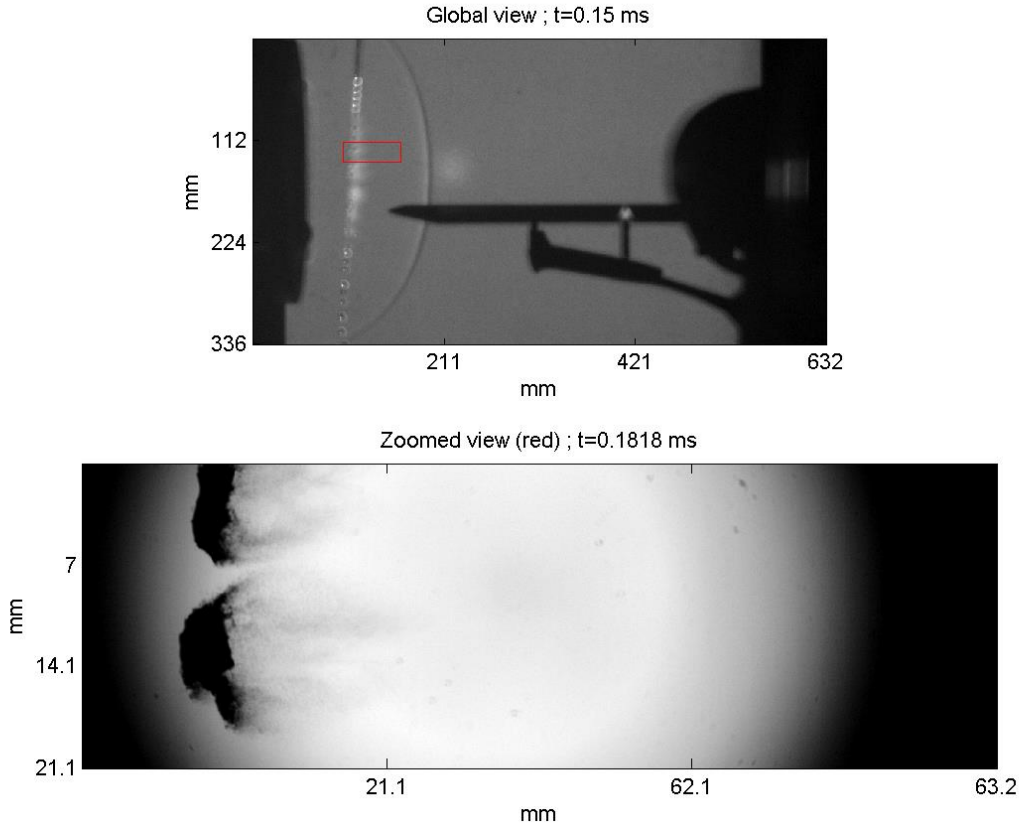

Fig. 12: Comparison of global and zoomed views

Fig.12 presents the two embedded synchronized views after shock wave interaction and the position of the zoomed view within the global view (red rectangle). The big cluster drop velocity in the horizontal direction is about 4m/s after the shock while the velocity of the secondary droplets is around 100m/s.

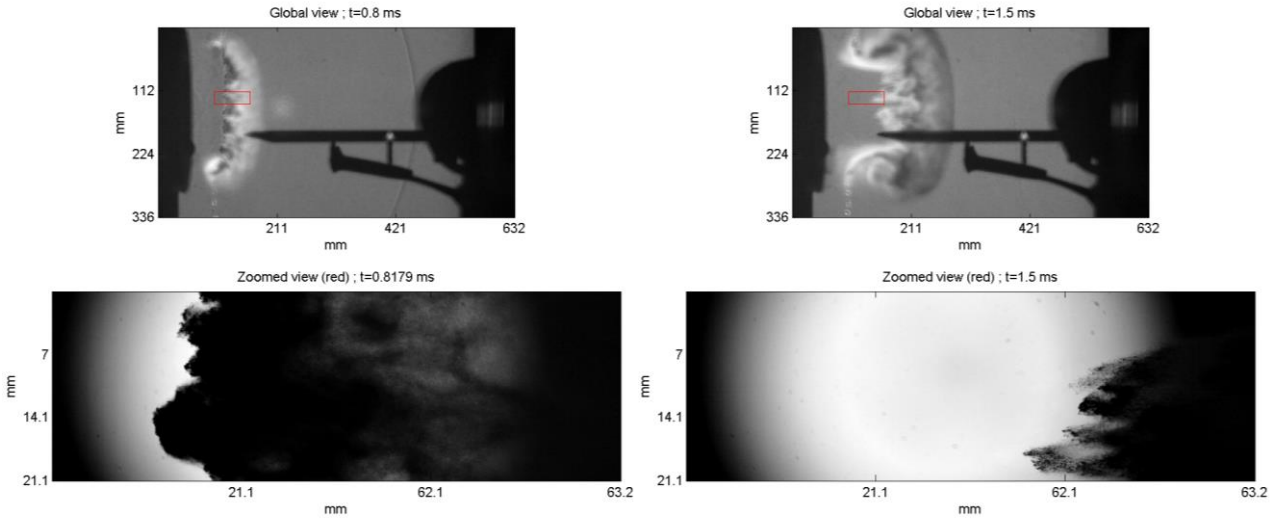

Fig. 13: Comparison of global and zoomed views at t=0.8ms and t=0.15ms

Composite movie has been generated and shows the evolution of both views with very nice images of the catastrophic breakup and droplets train interaction (Fig. 13). Moreover, in its full extent, this movie also shows the interaction of the drops debris with the secondary shocks from the first extremity of the tube and also with the blown wind (Fig.14).

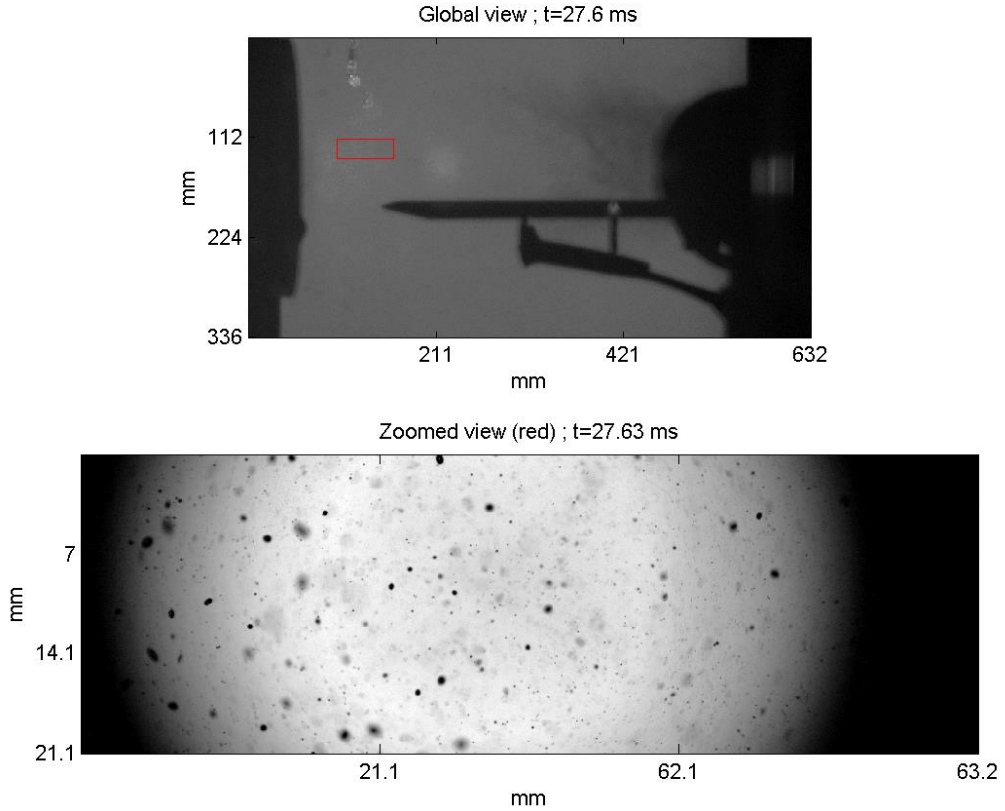

Fig. 14: Droplet debris: comparison of global and zoomed views at t=27.6ms

4.2 Conclusion and perspectives

We have shown the application of optical techniques to show the interaction of droplets with shock waves.
Pure in line shadowscopy is used to image the large area of interest of about $1m^2$ while direct shadowscopy with large zoom is used to image a smaller region of interest.
Time resolved measurements have been carried on to cope with high dynamics of the phenomenon under study. This has been achieved through coupling high speed CMOS camera with shadowscopic set-ups.
We have shown the catastrophic breakup of the droplet as the Weber number is very high for water droplets of about 3mm diameter in interaction with shock wave propagating around 400m/s. This works confirms some previous work from Gelfand [10] et al, but with higher time resolution thanks to the technical development of high speed imaging (cameras and light sources). We also enlarge the investigated ROI thanks to PILS configuration.
Next work will concern the study of different products and the change of atomization behavior following the Weber and Ohnesorge numbers. PIV measurements will be done on the drops debris.
For zoomed viewed, schlieren with PLIF light source [11] will be used to determine the velocities of droplet debris after catastrophic breakup, and also the droplet evaporation for some products such as Methyl Ethyl Ketone (MEK).

References

[1] Lecysyn, N., Dandrieux, A., Heymes, F., Aprin, L., Slangen, P., Munier, L., Le Gallic, C., Dusserre, G. (December 2009) Ballistic impact on an industrial tank: Study and modeling of consequences. *J. Hazard. Mat.*, 172(2–3), 30, pp 587-594.

[2] Krishna, K., Rogers, W.J., Mannan, M.S. (November 2003) The use of aerosol formation, flammability, and explosion information for heat-transfer fluid selection. *J. Hazard. Mat*., Vol. 104, Issues 1–3, 14, pp 215-226.
[3] Lecysyn, N., Dandrieux, A., Heymes, F., Slangen, P., Munier, L., Lapebie, E., Le Gallic, C., Dusserre, G. (2008) Preliminary study of ballistic impact on an industrial tank: Projectile velocity decay. *J. of Loss Prev. Process Ind.*, Vol. 21, Issue 6 November, pp 627-634.
[4] Slangen P., Heymes F., Aprin L., Munier L., Lapébie E., Dusserre G. (2012) Blast wave interaction with droplets: Time resolved measurements by laser shadowscopy. In: Proc. SPIE vol.8413, Vigo, Spain.
[5] Edgerton H. E. (1958) Shock wave photography of large subjects in daylight. *Rev. Sci. Instrum.* 29, pp 171–172.
[6] Settles G. S. (2001) Schlieren and Shadowgraph Techniques: Visualizing Phenomena in Transparent Media Springer-Verlag.
[7] Settles, G. S., Grumstrup, T. P., Miller, J. D., Hargather, M. J., Dodson, L. J., Gatto, J. A. (2005) Full-scale high-speed "edgerton" retroreflective shadowgraphy of explosions and gunshots. In: Proceedings of the 5th Pacific Symposium on Flow Visualization and Image Processing, Australia, September.
[8] Lee, C.H., Reitz, R. D. (February 2000) An experimental study of the effect of gas density on the distortion and breakup mechanism of drops in high speed gas stream. *Int. J. of Multiphase Flow*, Vol. 26, Issue 2, pp 229-244.
[9] Lin, S., Ruschak, K. (2004) Breakup of Liquid Sheets and Jets. *Appl. Mech. Rev*. doi:10.1115/1.1786591
[10] Gelfand, B. E. (1996) Droplet breakup phenomena in flows with velocity lag. *Progress in Energy Combustion Science*, 22(96), pp 201–265.
[11] Regert, T., Grossir, G., Paris, S., Luis Blay, E. (2014) Schlieren visualization for high-speed flows based on laser-induced fluorescence", *Exp Fluids* 55:1668, DOI 10.1007/s00348-014-1668-x